

Research article

Mohammad H. Tahersima^a, Zhizhen Ma^a, Yaliang Gui, Shuai Sun, Hao Wang, Rubab Amin, Hamed Dalir, Ray Chen, Mario Miscuglio and Volker J. Sorger*

Coupling-enhanced dual ITO layer electro-absorption modulator in silicon photonics

<https://doi.org/10.1515/nanoph-2019-0153>

Received May 24, 2019; revised July 21, 2019; accepted July 22, 2019

Abstract: Electro-optic signal modulation provides a key functionality in modern technology and information networks. Photonic integration has not only enabled miniaturizing photonic components, but also provided performance improvements due to co-design addressing both electrical and optical device rules. The millimeter to centimeter footprint of many foundry-ready electro-optic modulators, however, limits density scaling of on-chip photonic systems. To address these limitations, here we experimentally demonstrate a coupling-enhanced electro-absorption modulator by heterogeneously integrating a novel dual-gated indium-tin-oxide phase-shifting tunable absorber placed at a silicon directional coupler region. This concept allows utilizing the normally parasitic Kramers-Kronig relations here in a synergistic way resulting in a strong modulation depth to insertion loss ratio of about 1. Our experimental modulator shows a 2 dB extinction ratio for a just 4 μm short device at 4 V bias. Since no optical resonances are deployed, this device shows spectrally broadband operation as demonstrated here across the entire C-band. In conclusion, we demonstrate a modulator utilizing strong index change from both real and imaginary parts of active material enabling compact and high-performing modulators using semiconductor near-foundry materials.

^aMohammad H. Tahersima and Zhizhen Ma: contributed equally to this work.

*Corresponding author: Volker J. Sorger, George Washington University, 800 22nd Street NW, Washington, DC 20052, USA, e-mail: sorger@gwu.edu. <https://orcid.org/0000-0002-5152-4766>

Mohammad H. Tahersima, Zhizhen Ma, Yaliang Gui, Shuai Sun, Hao Wang, Rubab Amin and Mario Miscuglio: George Washington University, 800 22nd Street NW, Washington, DC 20052, USA. <https://orcid.org/0000-0002-9343-0557> (Z. Ma)

Hamed Dalir: Omega Optics, Inc., 8500 Shoal Creek Blvd., Bldg. 4, Suite 200, Austin, TX 78757, USA

Ray Chen: Department of Electrical and Computer Engineering, University of Texas at Austin, Austin, TX 78712, USA

Keywords: electro-absorption modulators; indium tin oxide; directional coupling; broadband operation.

1 Introduction

Integrated electro-optic (EO) modulators perform key applications in telecommunication [1], inter-chip and potentially intra (on-chip) photonic interconnections for multicore microprocessors and memory systems [2, 3], radio frequency and analog signal processing such as photonic analog to digital conversion [4, 5], and in sensors [6]. Monolithic integration, such as silicon photonics enables (i) densifying photonic networks compared to discretely packaged components, (ii) reduced device power consumption [7], and (iii) lower packaging costs. Due to the weak EO response of silicon [8], however, known monolithically integrated EO components have millimeter to centimeter footprint. The effort to miniaturize the monolithic EO components has been a major driver for the semiconductor industry over past decades [9]. Recent explorations in using photonic integrated circuits (PIC) for the interconnectivity functions of neural network also point to the importance of densification [10, 11].

The performance metrics for modulators [12, 13] are high speed (3 dB role-off, $f_{3\text{dB}}$) [14, 15], high sensitivity/energy efficiency (E/bit, dynamic power) [7, 16, 17], high extinction ratio (ER), and compact footprint (ER/unit-length) [15], and low insertion loss (IL). In order to achieve high-performance modulators, two possible routes can be followed: (i) increasing the light-matter interaction (LMI) such as increasing modal overlap, using optical resonances feedback (i.e. cavity Finesse, F), or utilizing a high-group index (slow light), and (ii) utilizing materials with strong optical index tunability [18]. On-chip plasmonic modulators (surface plasmonic or hybrid plasmonic waveguide) have been introduced as an efficient LMI enhancement approach due to the large group index in plasmonic mode, resulting in compact footprint and high-bandwidth devices [15, 19]. The significant ohmic

loss from plasmonic effect, however, limits the propagation distance of information encoded with light [20]. Thus, the modulation power efficiency suffers from optical power penalty [21]. On the other hand, silicon photonic micro-cavities with high quality (Q) factors were adopted to boost the LMI with photons interacting multiple times with the EO-tuned material proportional to the cavity's F [22], but the fundamental trade-off between the photon lifetime and device temporal response (f_{3dB}) constrains the modulator performance. Also, cavities with high Q would not operate in a broadband spectrum thus requiring thermal resonance tuning to match the desired wavelength used in the PIC, further increasing the modulation energy consumption via addition static power. To overcome the material limitation of silicon as EO "active" material, heterogeneous integration [23] has been introduced as a possible route to continue device scaling [12] while minimizing modulator signaling performance; the idea is to utilize the foundry-established silicon platforms for the passive waveguide parts for its low-loss propagation waveguide system, but to deploy other material options with stronger index modulation for active light manipulation. The weak index tuning of silicon, is due to (a) the low carrier induced plasma dispersion, and (b) the relatively low band gap. A variety of EO-functional materials, such as graphene [24, 25], III-V materials [26], and transparent conductive oxides (TCO) [27, 28] have been investigated for EO modulation. Here, we select indium-tin-oxide (ITO) as the EO material and integrate an ITO-oxide-ITO capacitive gate-stack atop a silicon photonic waveguide to form an all-photonic optical mode. The choice for ITO is four-fold: (i) the carrier concentration modulation in ITO can be in the order of $\sim 10^{20} \text{ cm}^{-3}$, which results in a refractive tuning in unity order [19, 27]; (ii) unity-strong optical index modulation ($\Delta n \sim 1$) has been experimentally observed at, or close to, the epsilon-near-zero (ENZ) condition [29, 30]; (iii) while process control of ITO has been challenging due to intrinsic material complexities, we have recently demonstrated a holistic (electrical and optical) approach to both precisely and repeatedly control ITO's parameters [31]; And (iv) ITO belongs to the class of TCO family and is currently used massively by both smart phones and the solar-cell industry for touch screens and transparent low-resistive front-end contact, respectively [32]. Hence, it might enter foundry processes sooner than other classically non-CMOS materials.

With the exceptional refractive index modulation, ITO has been heterogeneously integrated with photonic waveguide to build next-generation EO modulators. If using solely the imaginary part index tuning, with optimization of optical mode and material processing

condition, despite the material already gated to the ENZ point, a photonic electro-absorption (EA) ITO modulator has been reported to have only 0.15 dB/ μm ER [29], due to limited light-ITO thin film interaction. Recently, phase-shift-based ITO modulator has been also demonstrated by a Mach-Zehnder interferometer configuration [33], but the modulator performance is limited by fundamental Kramers-Kronig relation, thus either having a high IL, or exhibiting degraded ER as the loss and phase of the material changes simultaneously. With the addition of a photonic crystal cavity design, Wang's group demonstrated a nanocavity-based ITO modulator with ultracompact footprint [34]; the claim that for such a device is that the phase and absorption modulation of the material contribute coherently to the EO modulation. The concept of using both real and imaginary part index tunings for modulation is indeed interesting and actually an integral part of the novel coupling-enhanced EA modulation introduced in the work discussed in the this manuscript. Thus, we argue that for nanocavity-based devices, the extra absorption induced from ITO carrier accumulation would reduce the Q of the cavity thus broadening the spectrum response [35]. As a result, the overall ER of such modulator would be degraded by the extra loss accompanying the phase change of the material. Nevertheless, the aforementioned heterogeneously integrated ITO photonic modulators require silicon as a back gate, which usually has a low conductivity thus leads to high resistance-capacitance (RC) delay. Selective doping of silicon could be applied to reduce the serial resistance to achieve high-speed modulation, but increases the design and fabrication complexity and waveguide optical loss (i.e. IL).

Here, we experimentally demonstrate a compact coupling-enhanced dual-layer ITO modulator that uses both the real and imaginary parts of ITO's tunable index synergistically to increase EO modulation while not relying on optical or material resonances, thus allowing for spectrally broadband performance. In brief, in the absorptive state (light OFF) of the modulator, an additional waveguide section ("coupling island") in close proximity to the bus waveguide enables a higher ER compared to the traditional absorption-only case without sacrificing device footprint by realizing light power diversion (through coupling) away from the bus to the island (note, this light portion could be harvested by a photodetector for on-chip power generation). While in the light-ON state the coupling to the island is minimized, and the optical losses from absorption are also minimal due to the photonic (non-plasmonic) mode and dielectric-like dual-gated ITO/oxide/ITO stack atop of both waveguides (bus and island), thus enabling high optical transmission through the bus

waveguide. We experimentally achieve more than 2 dB of ER from a 4 μm short device (0.5 dB/ μm), benefiting from both the loss and coupling modulation of the system and low energy consumption of 0.77 pJ/bit. The nature of the directional coupling and free-carrier absorption from ITO enables a spectrally broadband response, which can be seamlessly integrated with wavelength division multiplexing technology for higher link-level data rates. Also, the dual stack ITO configuration eliminates the high serial resistance from silicon and thus enables a potentially short RC delay.

2 Results

For directional coupler (DC) devices, the study of an ITO-based directional switch was first introduced in 2015 [36], where a plasmonic mode and ITO/metal stack are placed on the bar waveguide to enhance the light-ITO interaction to realize large index mismatch between the bus and bar waveguide to control the coupling between waveguides. Also, unlike other phase change materials such as GeSbTe that could change from dielectric to metallic phase [37], the low mode overlap of the active region in such a photonic mode (ITO/silicon waveguide) would not provide a high effective index change for efficient switching (see Supplementary information iii). In contrast, in this work, we explore a different and thus far unexplored modulation

scheme by stacking ITO/oxide/ITO layers across both the bus and the coupling island to alter both the absorption and beating length of such a directional coupler (Figure 1). Without bias, the dual ITO layers are in flat band condition (assuming the same doping levels verified in ref [31], thus the ITO layers are in an optically low-loss state). Here, the DC's beating length is much longer than the island length resulting in high transmission at the bus waveguide (Figure 1A). By capacitively gating the dual ITO layers one achieves a higher linear absorption (loss) compared to the zero bias state due to carrier accumulation. Note that the dual-gated ITO layers being operated in a push-pull configuration might appear as if they only exhibit a small net index change (one ITO layer in carrier accumulation while the other in depletion). However, this is not true, since ITO's Drude model shows a non-symmetric index behavior with carrier concentration change (Figure 3A) [23]. In addition, the carrier accumulation greatly reduces the refractive index of ITO (order of unity) atop the waveguides and inside the gap (between both waveguides); thus, the optical path between two waveguides is reduced as, which is a similar effect as shrinking the gap between the bus and island waveguide. Since the coupling coefficient is rather sensitive to the gap size between the two waveguides, a higher optical power is transferred to the island waveguide with applied electrical bias, and a low transmission state from the bus waveguide can be observed (Figure 1B). Here, between the light ON

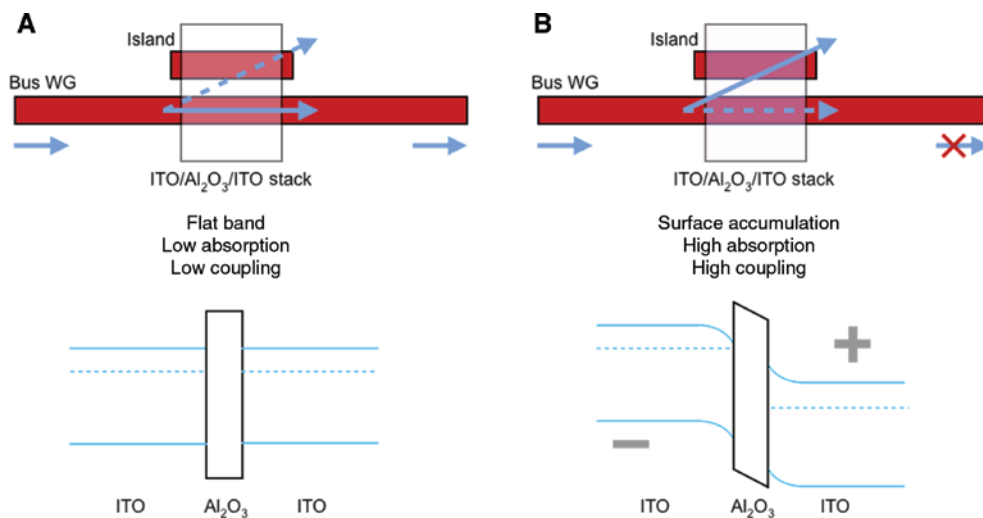


Figure 1: Operation principle for a coupling-enhanced ITO modulator; here the changes of both ITO absorption and coupling coefficient contribute synergistically to the modulation of the transmission on the bus waveguide, thus exploiting the Kramers-Kronig relations to achieve higher modulation performance as experimentally demonstrated in this work.

(A) Without external bias, the top and bottom layers of ITO have an intrinsically low carrier concentration, thus low absorption for the device region. Also, a long beating length prohibits coupling from the bus waveguide to the island waveguide; a high transmission could be expected from the bus waveguide. (B) With external gating applied, the bottom layer ITO becomes more absorptive due to carrier accumulation, while the beating length becomes shorter for the coupling region, and the transmission is blocked from the bus waveguide.

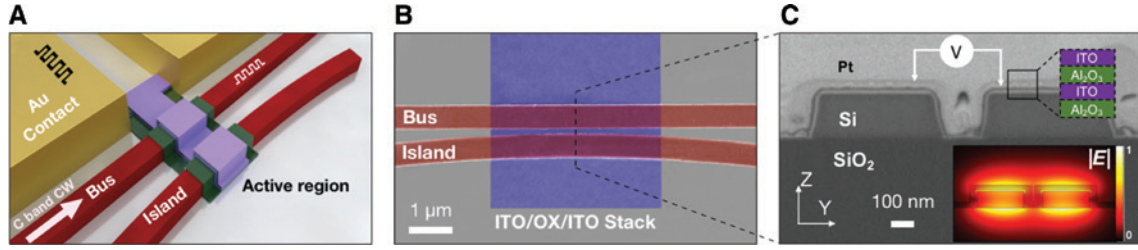


Figure 2: Device configuration of the coupling-enhanced modulator.

(A) Schematic of coupling-enhanced dual-gated ITO modulator. (B) Scanning electron microscopy image of fabricated device. (C) Cross-section image and mode profile illustrating the device layers and operating mechanism of the active region. An optical beam is modulated by modifying the coupling coefficient between bus and island waveguides via applying an electrical bias across the double ITO layer capacitor. In the coupling region, two waveguides are spaced by a gap distance $g=200$ nm, covered by an active stack (zoom-in: ITO/ Al_2O_3 /ITO). In the active coupling region, the first 10 nm of Al_2O_3 layer is directly deposited on top of the silicon waveguides as a passivation layer using atomic layer deposition (ALD), then the 15 nm inner ITO layer, 10 nm Al_2O_3 gate oxide, and 15 nm outer ITO layer is patterned and deposited on the coupling region consecutively to define the device region; the ITO layers are gated in a capacitively push-pull configuration to modulate the photonic coupler region. Here ITO's optical index changes nonlinearly (i.e. non-symmetrically z-direction) with applied bias (see Figure 3A). This nonlinear behavior is further enhanced by a non-symmetric model overlap of the bottom vs. top ITO-layer (the inset illustrates the corresponding TM mode-field profile from eigenmode analysis).

and OFF states, the synergistic usage of absorption and coupling, jointly (turned-on with bias) helps reducing the light transmission from the bus waveguide, hence increasing the obtainable modulator's ER. As an EO modulator, we claim that the real and imaginary part tunings of ITO contribute synergistically to the modulation depth (ER), and hence show that the Kramers-Kronig relations can be harnessed in a positive way.

Our dual-gated ITO modulator consists of a silicon photonic bus waveguide and a short (2–8 μm) coupling-island waveguide separated 200 nm away from the bus. Silicon-on-insulator (SOI) waveguides (width=500 nm, height=220 nm) are patterned via negative E-beam photoresist (hydrogen silsesquioxane) followed by dry etching using SF_6 and C_4F_8 , and the dual-gated Al_2O_3 /ITO/ Al_2O_3 /ITO stack is deposited on top of the coupling region, where the lower oxide serves as electrical isolation. Note that the short island waveguide is slightly curved away from the bus waveguide to minimize the abrupt effective index change for the propagation, thus minimizing the ILs from the SOI waveguide into the device section. Both ITO layers extend beyond the coupling region to facilitate electrical connection via two Ti/Au contact pads (Figure 2A). Overall, the 50 nm-tall (vertically) stack is not only on top of the waveguides, but also resides inside the gap between, which effects the propagating constant of the TM mode inside the waveguide (Figure 2C inset). This setup effectively allows voltage-tuning the coupled supermodes indices, hence altering the coupling length of the DC. The induced change in the carrier concentration of ITO layers thus tunes the absorption of ITO layers and the coupling factor between two waveguides simultaneously.

The optical permittivity of ITO, for near-infrared wavelength, can be described the Drude model as [27, 29]

$$\epsilon_{\text{ITO}}(\omega) = \epsilon_{\infty} - \frac{\omega_p^2}{\omega^2 + i\omega\Gamma} \quad (1)$$

where ω is the angular frequency of light, ϵ_{∞} is the high frequency permittivity of ITO, and Γ the damping frequency for the electron collisions inside ITO. And $\omega_p = \sqrt{\frac{N_c e^2}{\epsilon_0 m^*}}$ is the plasma frequency, depending on the carrier concentration N_c , and effective mass of electrons inside ITO film m^* . Thus, by changing the carrier concentration N_c in ITO electrically, the optical permittivity is tuned. It has been reported that for ITO deposition, depending on the processing and post-processing conditions, such as the gas mixture and temperature during sputter and post-annealing, the intrinsic carrier concentration could span from $1 \times 10^{19} \text{ cm}^{-3}$ to $1 \times 10^{21} \text{ cm}^{-3}$, which greatly affects the optical index for the as-deposited ITO film [38, 39]. In our work, we perform Hall-bar and ellipsometry measurement for our ITO thin films on a reference wafer which is processed in the same batch as the device sample, in order to control the ITO thin film optical property and extrapolate the carrier concentration and damping rate of the material. For instance, we measure an initial carrier concentration (without electrical bias) of $1.2 \times 10^{19} \text{ cm}^{-3}$ for our as-deposited ITO from Hall-bar measurement, which is rather low due to the absence of a post-deposition thermal treatment. Then broadband (193–1690 nm) ellipsometric spectroscopy is performed and fitted with the Lorentz oscillator, Cauchy model, and Drude model to extract the

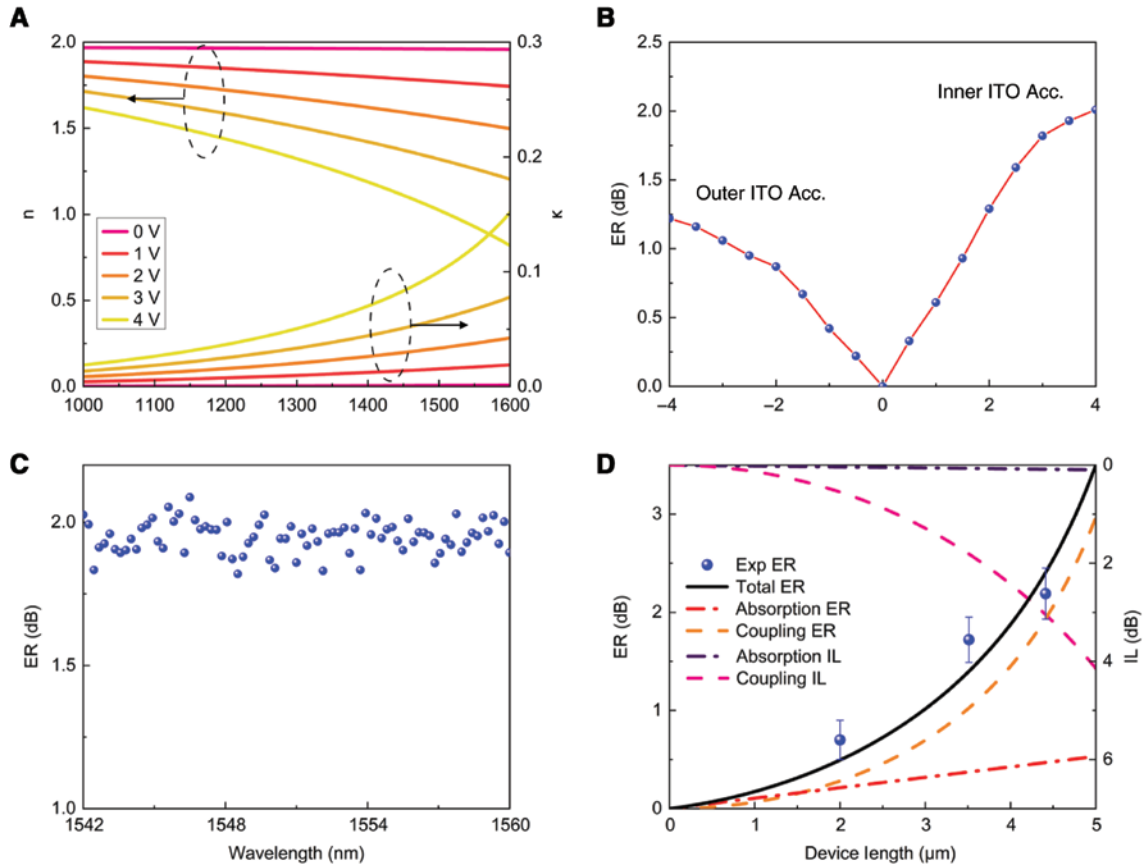


Figure 3: Simulated and experimental results for the ITO coupling-enhanced modulator.

(A) Experimental verified ITO refractive index data under different carrier concentrations, fitted using Drude model. (B) Modulation performance for a 4 μm device; note that for the outer layer ITO accumulation shows a weaker modulation effect compared to the inner ITO accumulation, since it is further away to the waveguide core. (C) Broadband performance of the modulator across C band; the limitation is mainly due to the spectrum response of the grating coupler. (D) Length-dependent measurement for three different device lengths (2 μm , 4 μm , and 6 μm long devices have been fabricated and measured, which correspond to an effective coupling device length (since the coupling island waveguide section is bend to reduce waveguide coupling losses into the modulator section) of 1.95 μm , 3.4 μm and 4.4 μm , respectively) shows a good agreement with the numerical simulation result, illustrating the contribution of linear absorption and coupling change for the ER. The contribution from absorption and coupling to IL is also plotted explicitly; a stronger contribution from coupling is found.

ITOs film parameters at zero bias giving a damping rate of 9.5×10^{13} rad/s, at the lowest mean square error [31]. Fabricated devices (with the 10 nm Al_2O_3 gate oxide) show an ITO carrier concentration in the accumulation layer of 5.1×10^{20} cm^{-3} for 4 V electrical bias, while the optical property of ITO with carrier concentration is plotted in Figure 3A; for 1550 nm wavelength in our device the accumulation layer of ITO is tuned to be close to ENZ point ($\sim 6.8 \times 10^{20}$ cm^{-3}), achieving nearly unity change in the real part of the refractive index and a significant increase in optical loss (κ) of the ITO film. In addition, an analysis of the ITO's accumulation layer carrier concentration profile could be implemented using the modified Thomas-Fermi approximation (MTFA) method to allow for the quantum-mechanical influence of an infinite potential barrier at the surface, and it has shown compliance for semiconductors

with surface band bending at nanoscale [40]. For ITO, the modified Thomas-Fermi approximate screening length λ_{MTFA} was found to be $\sim 3\text{nm}$ [40]. With MTFA, the carrier density change in our ITO accumulation is found to be $\Delta N_c = 2.5 \times 10^{21}$ cm^{-3} , indicating an even stronger permittivity change beyond the ENZ point.

Given the slight curvature of the coupling island relative to the waveguide bus, the effective coupling length is shorter than the physical lateral size of the stack; for instance, for the 4 μm long active device region, this effective coupler length is actually 3.4 μm after normalization to a straight coupler with 200 nm gap size. Without bias both ITO layers exhibit dielectric material property with low loss. Performing a 2D eigenmode analysis, we find the effective index difference (phase mismatch) between the first order and second order modes to be 0.099, with a

low linear absorption of $\alpha = 21.89 \text{ cm}^{-1}$ (see Supplementary information iv). The DC coupler's beating length in this case can be estimated by

$$L_{\text{beat}} = \frac{\lambda}{2(n_{\text{even}} - n_{\text{odd}})} \approx 7.8 \text{ } \mu\text{m} \quad (2)$$

where $\lambda = 1.55 \text{ } \mu\text{m}$ is the operating wavelength, yielding an IL of 2.1 dB for this 4 μm long device at ON state. With applied bias of 4 V (i.e. inner ITO layer biased to accumulation), the stronger free-carrier absorption from ITO increases the linear absorption of the supermode to be $\alpha = 146 \text{ cm}^{-1}$. Meanwhile, the near-unity index reduction of ITO's real part reduces the effective optical path between the bus and island waveguide, resulting in an increased phase mismatch between the first and second order mode of 0.117, consecutively corresponding to a shorter beating length of 6.6 μm . Thus, more optical energy transfers from the bus to the island waveguides while the increased absorption simultaneously further decreases the transmission of the bus waveguide compared to the ON state. Thus, the increased coupling coefficient from real index modulation and higher free-carrier absorption accompanying the real index change contribute simultaneously to the intensity modulation on the bus waveguide, resulting in an ER = 2 dB for this 4 μm -short modulator. Interestingly, we observe a weaker modulation when the outer ITO layer is in accumulation state, which is due to the outer ITO being further away from the silicon waveguide core, resulting in a lower ITO mode overlap and thus smaller effective index change for the coupled mode (Figure 3B). Also, the modulator performance is measured to be quite uniform across the C-band, because of the non-resonant nature of both the coupling effect and the intra-band free-carrier-based absorption from ITO (Figure 3C). Lastly, the length-dependent study of effective (i.e. bending-corrected) coupling length versus ER performance shows reasonable agreement between the numerical approach and experimental measurement (Figure 3D). This indicates that indeed the change of linear absorption and coupling coefficient contribute synergistically towards higher ER.

In addition to the joint contribution from both the real and imaginary index change towards a mutually synergistic modulation operation, the dual-gated ITO layer also supports overcoming the high serial resistance drawbacks of devices where ITO is biased against silicon [33, 34]. Providing some estimation to this effect here, for our 4 μm device, the metal contacts are spaced 6 μm away from the active region, and thus the serial resistance is 1.8 K Ω using our measured resistivity of deposited ITO thin film of $1.8 \times 10^{-5} \text{ } \Omega \cdot \text{m}$ from Hall bar measurement, which is even

a few times lower than those reported for doped silicon waveguide as the contact [34]. The estimated RC limited bandwidth of our device is 458 MHz, with a capacitance of 193 fF. However, with proper optimization such as reducing contact spacing of the device region, both the serial resistance and capacitance could be reduced to 525 Ω and 56 fF, respectively, which corresponds to a RC bandwidth of 5.4 GHz and modulation energy consumption of 200 fJ/bit, while keeping a minimum distance of half a wavelength (750 nm) to avoid generating plasmonic effect (see Supplementary information v). Overall, with 2 dB modulation from a 4 μm -compact device, such a modulation of 0.5 dB/ μm is rather high compared to other device schemes and does not even rely on resonances (spectrally broadband). With an IL = 2 dB, the ER/IL-ratio is about unity; while this is not outstanding compared to lithium-niobate [41] or even silicon [21] modulators, these devices are 3–4 orders of magnitude more compact. Also, engineering the device dimension, for instance, reducing the gap size to below 200 nm or increasing the device length to reach 2 times the beating length at ON state, would further enhance the ER/IL performance of the device while keeping the device footprint still in sub-20 μm range, which is much shorter than a linear absorption-only ITO modulator [29, 42] (see Supplementary information vi). This way, an ER/IL ratio of 7 (3.5 dB/0.5 dB) could be achieved with the tradeoff of a longer device length (~16 μm).

3 Conclusion

In summary, we introduce and experimentally demonstrate a novel coupling-enhanced dual-gated ITO modulator heterogeneously integrated at the coupling regime between a silicon waveguide bus and a short coupling island. We show that for our coupling-enhanced electro-absorption modulator, both the real and imaginary index modulation of this ITO/oxide/ITO stack synergistically contribute towards the modulation, thus exploiting the Kramers-Kronig relations synergistically. This way we experimentally achieve a 2 dB ER modulation while being 4 μm compact (0.5 dB/ μm) with an IL of 2 dB (ER/IL = 1) for 4 V of applied bias. We verify a flat spectral response across the C-band frequencies since neither optical nor material resonances are needed in this device configuration. The design features careful process control to enable an ITO material away from the ENZ point at light ON state to reduce losses while demonstrating a near-unity ITO EO index change under modulation. Taken together, the heterogeneous integration of an emerging EO material, ITO, which is commonly used in the semiconductor industry,

offers positive device synergies demonstrating a compact coupling-enhanced modulator on a silicon photonic platform [43].

Acknowledgments: VS is funded by AFOSR (FA9550-17-1-0377) and ARO (W911NF-16-2-0194) and HD by NASA STTR, Phase I (80NSSC18P2146).

References

- [1] Barwicz T, Watts M, Popovi M, et al. Polarization-transparent microphotonic devices in the strong confinement limit. *Nat Photonics* 2007;1:57–60.
- [2] Batten C, Joshi A, Orcutt J, et al. Building many-core processor-to-DRAM networks with monolithic CMOS silicon photonics. *IEEE Micro* 2009;29:8–21.
- [3] Green WM, Rooks MJ, Sekaric L, Vlasov YA. Ultra-compact, low RF power, 10 Gb/s silicon Mach-Zehnder modulator. *Opt Express* 2007;15:17106.
- [4] Holzwarth CW, Amatya R, Araghchini M, et al. High speed analog-to-digital conversion with silicon photonics. In: *Silicon Photonics IV*, Vol. 7220. Bellingham, WA, USA, International Society for Optics and Photonics, 2009, 72200B.
- [5] Li A, Singh S, Sievenpiper D. Metasurfaces and their applications. *Nanophotonics* 2018;7:989–1011.
- [6] Kim GD, Lee H, Park C, et al. Silicon photonic temperature sensor employing a ring resonator manufactured using a standard CMOS process. *Opt Express* 2010;18:22215.
- [7] Timurdogan E, Sorace-Agaskar C, Sun J, Shah Hosseini E, Biberman A, Watts M. An ultralow power athermal silicon modulator. *Nat Commun* 2014;5:4008.
- [8] Soref R, Bennett B. Electrooptical effects in silicon. *IEEE J Quantum Elect* 1987;23:123–9.
- [9] Liu A, Jones R, Liao L, et al. A high-speed silicon optical modulator based on a metal-oxide-semiconductor capacitor. *Nature* 2004;427:615–8.
- [10] Heuser T, Große J, Kaganskiy A, Brunner D, Reitzenstein S. Fabrication of dense diameter-tuned quantum dot micropillar arrays for applications in photonic information processing. *APL Photon* 2018;3:116103.
- [11] Miscuglio M, Mehrabian A, Hu Z, et al. All-optical nonlinear activation function for photonic neural networks [Invited]. *Opt Mater Express* 2018;8:3851.
- [12] Liu K, Sun S, Majumdar A, Sorger VJ. Fundamental scaling laws in nanophotonics. *Sci Rep* 2016;6:37419.
- [13] Amin R, Khurgin JB, Sorger VJ. Waveguide-based electro-absorption modulator performance: comparative analysis. *Opt Express* 2018;26:15445.
- [14] Dalir H, Xia Y, Wang Y, Zhang X. Athermal broadband graphene optical modulator with 35 GHz speed. *ACS Photon* 2016;3:1564–8.
- [15] Haffner C, Heni W, Fedoryshyn Y, et al. All-plasmonic Mach-Zehnder modulator enabling optical high-speed communication at the microscale. *Nat Photon* 2015;9:525–8.
- [16] Sorger VJ, Amin R, Khurgin JB, Ma Z, Dalir H, Khan S. Scaling vectors of attojoule per bit modulators. *J Optics* 2018;20:014012.
- [17] Amin R, Ma Z, Maiti R, et al. Attojoule-efficient graphene optical modulators. *Appl Optics* 2018;57:D130.
- [18] Ma Z, Tahersima MH, Khan S, Sorger VJ. Two-dimensional material-based mode confinement engineering in electro-optic modulators. *IEEE J Sel Top Quantum Electron* 2017;23:81–8.
- [19] Sorger VJ, Lanzillotti-Kimura ND, Ma RM, Zhang X. Ultra-compact silicon nanophotonic modulator with broadband response. *Nanophotonics* 2012;1:17–22.
- [20] Khurgin JB. How to deal with the loss in plasmonics and metamaterials. *Nat Nanotechnol* 2015;10:2–6.
- [21] Li G, Krishnamoorthy A, Shubin I, et al. Ring resonator modulators in silicon for interchip photonic links. *IEEE J Sel Top Quantum Electron* 2013;19:95–113.
- [22] Xu Q, Schmidt B, Pradhan S, Lipson M. Micrometre-scale silicon electro-optic modulator. *Nature* 2005;435:325–7.
- [23] Amin R, Suer C, Ma Z, et al. Active material, optical mode and cavity impact on nanoscale electro-optic modulation performance. *Nanophotonics* 2017;7:455–72.
- [24] Liu M, Yin X, Zhang X. Double-layer graphene optical modulator. *Nano Lett* 2012;12:1482–5.
- [25] Ansell D, Radko I, Han Z, Rodriguez F, Bozhevolnyi S, Grigorenko A. Hybrid graphene plasmonic waveguide modulators. *Nat Commun* 2015;6:8846.
- [26] Hiraki T, Aihara T, Hasebe K, et al. Heterogeneously integrated III-V/Si MOS capacitor Mach-Zehnder modulator. *Nat Photonics* 2017;11:482–5.
- [27] Feigenbaum E, Diest K, Atwater HA. Unity-order index change in transparent conducting oxides at visible frequencies. *Nano Lett* 2010;10:2111–6.
- [28] Kinsey N, DeVault C, Kim J, Ferrera M, Shalae V, Boltasseva A. Epsilon-near-zero Al-doped ZnO for ultrafast switching at telecom wavelengths. *Optica* 2015;2:616.
- [29] Liu X, Zang K, Kang JH, et al. Epsilon-near-zero Si slot-waveguide modulator. *ACS Photon* 2018;5:4484–90.
- [30] Lee HW, Papadakis G, Burgos S, et al. Nanoscale conducting oxide PlasMOStor. *Nano Lett* 2014;14:6463–8.
- [31] Gui Y, Miscuglio M, Ma Z, et al. Towards integrated metatronics: a holistic approach on precise optical and electrical properties of indium tin oxide. *arXiv preprint arXiv:1811.08344v4* (2019).
- [32] Fortunato E, Ginley D, Hosono H, Paine DC. Conducting oxides for photovoltaics. *MRS Bull* 2007;32:6.
- [33] Amin R, Maiti R, Carfano C, et al. 0.52 V mm ITO-based Mach-Zehnder modulator in silicon photonics. *APL Photon* 2018;3:126104.
- [34] Li E, Gao Q, Chen RT, Wang AX. Ultracompact silicon-conductive oxide nanocavity modulator with 0.02 lambda-cubic active volume. *Nano Lett* 2018;18:1075–81.
- [35] Li E, Nia BA, Zhou B, Wang AX. Transparent conductive oxide-gated silicon microring with extreme resonance wavelength tunability. *Photon Res* 2019;7:473.
- [36] Ye C, Liu K, Soref RA, Sorger VJ. A compact plasmonic MOS-based 2 × 2 electro-optic switch. *Nanophotonics* 2015;4:261–8.
- [37] Xu P, Zheng J, Doyle JK, Majumdar A. Low-loss and broadband nonvolatile phase-change directional coupler switches. *ACS Photon* 2019;6:553–7.
- [38] Michelotti F, Dominici L, Descrovi E, Danz N, Menchini F. Thickness dependence of surface plasmon polariton dispersion

- in transparent conducting oxide films at 155 μm . *Opt Lett* 2009;34:839.
- [39] Ma Z, Li Z, Liu K, Ye C, Sorger VJ. Indium-tin-oxide for high-performance electro-optic modulation. *Nanophotonics* 2015;4:198–213.
- [40] Liu X, Kang J, Yuan H, et al. Tuning of plasmons in transparent conductive oxides by carrier accumulation. *ACS Photon* 2018;5:1493–8.
- [41] Wang C, Zhang M, Chen X, et al. Integrated lithium niobate electro-optic modulators operating at CMOS-compatible voltages. *Nature* 2018;562:101–4.
- [42] Amin R, Suer C, Ma Z, et al. A deterministic guide for material and mode dependence of on-chip electro-optic modulator performance. *Solid-State Electronics* 2017;136:92–101.
- [43] Narayana VK, Sun S, Badawy AHA, Sorger VJ, El-Ghazawi T. MorphoNoC: exploring the design space of a configurable hybrid NoC using nanophotonics. *Microprocess Microsy* 2017;50:113–26.

Supplementary Material: The online version of this article offers supplementary material (<https://doi.org/10.1515/nanoph-2019-0153>).